

A group of ductile metallic glasses prepared by modifying local structure of icosahedral quasicrystals

Qi Qiao(乔琪), Ji Wang(王吉), Zhengqing Cai(蔡正清), Shidong Feng(冯士东), Zhenqiang Song(宋贞强), Benke Huo(霍本科), Zijing Li(李子敬), and Li-Min Wang(王利民)
Citation: Chin. Phys. B, 2023, 32 (**11**): 116401. DOI: 10.1088/1674-1056/ace823
Journal homepage: http://cpb.iphy.ac.cn; http://iopscience.iop.org/cpb

What follows is a list of articles you may be interested in

Crystallization evolution and relaxation behavior of high entropy bulk metallic glasses using microalloying process

Danhong Li(李丹虹), Changyong Jiang(江昌勇), Hui Li(栗慧), and Mahander Pandey
Chin. Phys. B, 2021, 30 (**6**): 066401. DOI: 10.1088/1674-1056/abd92c

Internal friction behavior of $Zr_{59}Fe_{18}Al_{10}Ni_{10}Nb_3$ metallic glass under different aging temperatures

Israa Faisal Ghazi, Israa Meften Hashim, Aravindhan Surendar, Nalbiy Salikhovich Tuguz, Aseel M. Aljeboree, Ayad F. Alkaim, and Nisith Geetha
Chin. Phys. B, 2021, 30 (**2**): 026401. DOI: 10.1088/1674-1056/abc14f

Thermal effects and evolution of the defect concentration based on shear modulus relaxation data in a Zr-based metallic glass

Qi Hao(郝奇), Ji-Chao Qiao(乔吉超), E V Goncharova, G V Afonin, Min-Na Liu(刘敏娜), Yi-Ting Cheng(程怡婷), V A Khonik
Chin. Phys. B, 2020, 29 (**8**): 086402. DOI: 10.1088/1674-1056/ab969c

Effect of Sn and Al additions on the microstructure and mechanical properties of amorphous Ti-Cu-Zr-Ni alloys

Fu-Chuan Chen(陈福川), Fu-Ping Dai(代富平), Xiao-Yi Yang(杨霄熠), Ying Ruan(阮莹), Bing-Bo Wei(魏炳波)
Chin. Phys. B, 2020, 29 (**6**): 066401. DOI: 10.1088/1674-1056/ab8628

Effect of Ni substitution on the formability and magnetic properties of $Gd_{50}Co_{50}$ amorphous alloy

Ben-Zheng Tang(唐本镇), Xiao-Ping Liu(刘晓萍), Dong-Mei Li(李冬梅), Peng Yu(余鹏), Lei Xia(夏雷)
Chin. Phys. B, 2020, 29 (**5**): 056401. DOI: 10.1088/1674-1056/ab7da8

A group of ductile metallic glasses prepared by modifying local structure of icosahedral quasicrystals

Qi Qiao(乔琪)[1], Ji Wang(王吉)[1], Zhengqing Cai(蔡正清)[1], Shidong Feng(冯士东)[1,3], Zhenqiang Song(宋贞强)[1], Benke Huo(霍本科)[1], Zijing Li(李子敬)[2,†], and Li-Min Wang(王利民)[1,‡]

[1] *State Key Laboratory of Metastable Materials Science and Technology, School of Materials Science and Engineering, Yanshan University, Qinhuangdao* 066004, *China*

[2] *Key Laboratory for Microstructural Material Physics of Hebei Province, School of Science, Yanshan University, Qinhuangdao* 066004, *China*

[3] *Hebei Key Laboratory for Optimizing Metal Product Technology and Performance, Yanshan University, Qinhuangdao* 066004, *China*

(Received 22 May 2023; revised manuscript received 14 July 2023; accepted manuscript online 18 July 2023)

Inspired by research into the association between icosahedral local orders and the plasticity of metallic glasses (MGs), beryllium (Be) is added to the icosahedral quasi-crystal forming alloy $Zr_{40}Ti_{40}Ni_{20}$. In this way, bulk metallic glasses (BMGs) with favorable compressive plasticity are fabricated. Therein, the icosahedral quasi-crystalline phase is the main competing phase of amorphous phases and icosahedral local orders are the main local atomic motifs in amorphous phases. The alloys of $(Zr_{40}Ti_{40}Ni_{20})_{76}Be_{24}$ and $(Zr_{40}Ti_{40}Ni_{20})_{72}Be_{28}$ with their greater plastic strain capacity show similar characteristics to highly plastic amorphous systems: The serrated flow of compression curves always follows a near-exponential distribution. The primary and secondary shear bands intersect each other, bifurcate, and bend. Typical vein patterns are densely distributed on the fracture surfaces. The relaxation enthalpy of four MGs is linearly correlated with the plastic strain, that is, the greater the relaxation enthalpy, the larger the plastic strain.

Keywords: metallic glass, glass formation, compressive plasticity, relaxation enthalpy

PACS: 64.70.pe, 46.35.+z, 82.56.Na **DOI:** 10.1088/1674-1056/ace823

1. Introduction

Metallic glasses (MGs), as novel materials, have unique and excellent physical, chemical, and mechanical properties such as outstanding elasticity (2% strain at the elastic limit), high strength, good wear resistance, high corrosion resistance, and excellent soft magnetic performance, due to their particular structures.[1–6] These excellent properties impart potential applications to MGs. However, MGs do not contain defects such as dislocations and grain boundaries as those in crystals, so they fails to dissipate externally applied energy. As a result, MGs show poor plasticity and are likely to suffer disastrous brittle fracture under external loads.[7–10] Brittle fracture limits applications of metallic glasses as structural materials. Considering the fundamental influences of shear bands on plasticity of MGs, many methods of optimizing the plasticity of MGs by regulating the density of shear bands have been proposed, including shear band limitation,[11] shot peening,[12] and nanocrystalline recombination.[13] Thus, exploring bulk MGs with high plasticity has long been key to research into such amorphous materials.[14,15]

Previous research indicated that structural inhomogeneity in MGs is the structural origin of plastic deformation.[16–18] The icosahedral local orders produce structural inhomogeneity in amorphous alloys and are conducive to improving the plasticity of such amorphous alloys.[19–25] Such MGs containing icosahedral local orders generally show two-step crystallization behaviors, in which the primary crystalline phase is quasi-crystalline phase.[26–28] Inspired by this, if bulk amorphous alloys can be prepared by modulating structures of quasi-crystalline systems through doping, it is possible that local orders of MGs are dominated by icosahedral local orders. In this way, amorphous alloys with excellent plasticity can be obtained. Based on an icosahedral quasi-crystal-forming system $Zr_{40}Ti_{40}Ni_{20}$,[29] four bulk MGs $(Zr_{40}Ti_{40}Ni_{20})_{100-x}Be_x$ ($x = 20$, 24, 28, 32) were designed and fabricated by doping beryllium (Be). In the formula of $(Zr_{40}Ti_{40}Ni_{20})_{100-x}Be_x$, the ratios of the elements are molar percentages. In the subsequent expressions used herein, all components $(Zr_{40}Ti_{40}Ni_{20})_{80}Be_{20}$ are abbreviated to Be20%, the rod of $(Zr_{40}Ti_{40}Ni_{20})_{80}Be_{20}$ with diameter of 2 mm are abbreviated to Be20%-2 mm, and so on. The results show that, in the solidification process, the quasi-crystalline phase is the only competing phase of the amorphous phase, which indicates that icosahedral local orders are the main local structures in MGs. Addition of Be can significantly increase icosahedral local orders in the alloy systems, especially the fraction of distorted icosahedral local orders. The bulk MGs formed by use of such a quasi-crystalline doping method exhibit high compressive plasticity, in which the compressive plastic strains of both MGs Be24% and Be28% exceeds 10%. Moreover, all MGs can be work-hardened.

†Corresponding author. E-mail: lizijing_sh@163.com

‡Corresponding author. E-mail: Limin_Wang@ysu.edu.cn

© 2023 Chinese Physical Society and IOP Publishing Ltd

2. Experimental work

As described in our earlier studies,[30] homogeneous ingots of $(Zr_{40}Ti_{40}Ni_{20})_{100-x}Be_x$ ($x = 0$, 20, 24, 28, 32) were prepared by melting mixtures of high-purity elements (>99.9 wt%) five times under an Ar atmosphere in an arc-melting furnace. The copper mold suction casting method was used to prepare alloy rods with different sizes. The nature and microstructure of the samples were determined by x-ray diffraction (XRD) with Cu K_α radiation (Shimadzu XRD-6000) and transmission electron microscopy (TEM) using a JEOL-100FX microscope. Thermal analysis of the glassy samples was performed using a differential scanning calorimeter (PE DSC8000) at a heating rate of 2 K/min in a flowing argon atmosphere. Uniaxial compression tests were conducted on Instron-5982 at room temperature under a strain rate of 7.5×10^{-4} s^{-1}. The test samples were cylinders with a length of 4 mm and a diameter of 2 mm. The fractured samples were examined by using a scanning electron microscope (SEM).

3. Results and discussions

Figure 1(a) displays the XRD spectra of as-cast alloy rods with diameter of 2 mm for each of the alloys $(Zr_{40}Ti_{40}Ni_{20})_{100-x}Be_x$ ($x = 20$, 24, 28, 32). There are only amorphous diffraction peaks visible in the XRD spectra of the samples, indicating their completely amorphous nature. To check whether icosahedral quasi-crystals are the main competitor against the amorphous phase, the alloys were cast into rods with diameters exceeding the critical values. The glass-only rod of Be28% was annealed for four hours at a temperature of 680 K ($T_g + 40$ K), the samples were then subjected to XRD analysis to verify the *in situ* precipitated crystalline phase and the initial crystalline phase of alloy rods (Fig. 1(b)). Except for the XRD result of the alloy Be32%, all the XRD patterns contain only three main diffraction peaks, which are unique XRD patterns for icosahedral quasicrystals. Referring to Chan's indexing scheme, the three peaks can be respectively indexed as 18/29, 20/32, and 52/84.[31–33] The XRD results suggest that except the *in situ* precipitated crystalline phases in the sample of Be32%-15 mm are other stable crystalline phases, both the *in situ* precipitated, and initial crystalline phases in all alloys are quasi-crystalline. This result indicates that, for Be contents of no more than 28%, the quasi-crystal is always the main competing phase against the amorphous phase. This finding was further proved by the experimental results arising from transmission electron microscopy (TEM) as applied to the Be20%-15 mm and Be24-20 mm alloys. Figures 1(c) and 1(d) present the TEM bright-field images of Be16%-5 mm and Be20%-15 mm. Symbols Q and A in the figure denote the quasi-crystalline grain and amorphous regions, respectively. Figure 1(e) displays the TEM high-resolution images of region Q in Be20%-15 mm, in which the intact and distorted icosahedral atomic configurations indicate its quasi-crystalline nature. The quasi-crystalline properties can be further verified by the two-, three-, and five-fold symmetries in the electron diffraction patterns of the region Q as shown in Fig. 1(f), which are typical of icosahedral quasi-crystals. In the region denoted by A, the electron diffraction results are typical of amorphous halo rings. It is evident that, compared with the ally sample Be16%-5 mm, the quasi-crystalline grains of the Be24%-15 mm specimens are smaller. Given that the Be20%-15 mm specimens prepared shows a lower cooling rate, smaller quasi-crystalline grains of Be20%-15 mm engender greater difficulty in the crystallization of quasi-crystals. Meanwhile, as

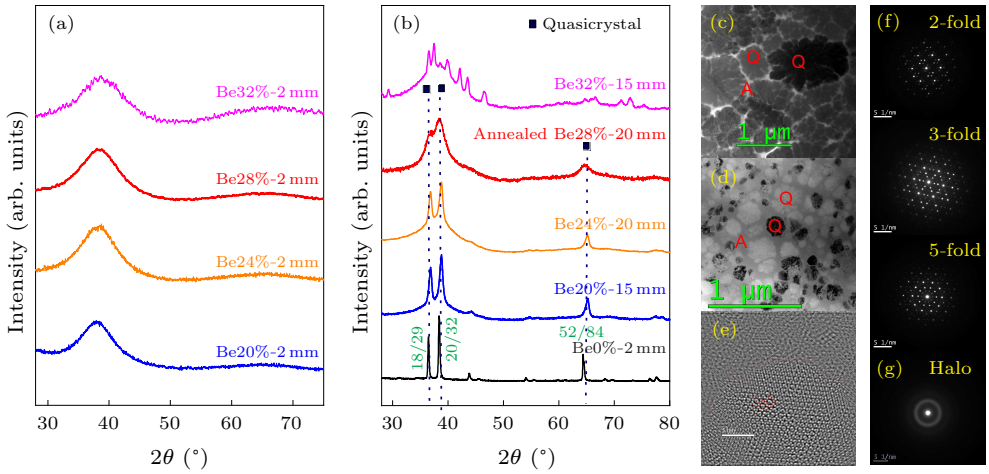


Fig. 1. (a) XRD patterns of the as-cast alloy rods with diameter of 2 mm in alloys $(Zr_{40}Ti_{40}Ni_{20})_{100-x}Be_x$ ($x = 20$, 24, 28, 32); (b) XRD patterns of the as-cast rods with different diameters in alloys of $(Zr_{40}Ti_{40}Ni_{20})_{100-x}Be_x$ ($x = 0$, 20, 24, 28, 32), among which the XRD spectra of the sample of $(Zr_{40}Ti_{40}Ni_{20})_{72}Be_{28}$ annealed at a temperature of 690 K are also included; (c) TEM bright-field images of the as-cast rod with diameter of 5 mm for the alloy $(Zr_{40}Ti_{40}Ni_{20})_{84}Be_{16}$; (d) TEM bright-field images of the as-cast rod with diameter of 15 mm for the alloy $(Zr_{40}Ti_{40}Ni_{20})_{80}Be_{20}$; (e) high-resolution TEM images of the as-cast rod with diameter of 15 mm for the alloy $(Zr_{40}Ti_{40}Ni_{20})_{80}Be_{20}$; (f) and (g) electron diffraction images of the selected zones denoted by Q and A in (c) for the $(Zr_{40}Ti_{40}Ni_{20})_{80}Be_{20}$ suction-cast rod with diameter of 15 mm.

quasi-crystals are the main competing phase against non-crystals, higher difficulty in crystallization of quasi-crystals indicates a higher glass formability. This result was in line with the earlier reported study[30] in that, with the increased Be content, the critical glassy size increases from 2 mm for the alloy Be20%, to 15 mm for the alloy Be24%, to the peak value of 20 mm for the alloy Be28%, and then drops to 12 mm for alloy Be32%.

Figure 2(a) shows the uniaxial compressive stress-strain curves of four complete MG rods with diameter 2 mm of Be20%, Be24%, Be28% and Be32% at room temperature. The aspect ratios of the four samples were all set to 2:1. Experimental results imply that these systems, when subjected to external load, demonstrate favorable compressive plasticity. Meanwhile, each sample shows similar work-hardening. Among the four systems, as the Be content is increased, the yield strength of the amorphous alloy is reduced; the plastic deformation capacity increases, then decreases. The amount of plastic deformation for amorphous alloy Be24 at.% is the largest (at 13.35%); when the Be content reaches 32 at.%, the plastic deformation capacity and yield strength of amorphous alloy both decrease significantly: the yield strength is only 1351 MPa and the amount of plastic deformation is only 5.6%. Uniaxial compression test data pertaining to the alloy specimens are displayed in Table 1. Figure 2(b) illustrates the serrated flow behavior of amorphous alloy Be24%-2 mm when the strain is about 10%. Such behavior of Be24%-2 mm is relatively complex, encompassing stress drops of variable magnitude. This is akin to the serrated flow behavior of largely plastic MGs as previously reported.[34] Statistics pertaining to serrated flow behavior of the strain-stress curves for the four alloys are related to those in the literature.[34] Figures 2(c) and 2(d) present the distribution histograms of the magnitude of the stress drop for amorphous alloys Be20%-2 mm, Be24%-2 mm, Be28%-2 mm, and Be32%-2 mm. The lateral axis s denotes the decreasing amplitude of reduced stress in the serrated flow curves; and the longitudinal axis $N(s)$ represents the number of stress drops corresponding to the decreasing amplitude of reduced stress s. The results indicate that all of the serrated flows of the four MGs show near-exponential distribution characteristics. Noticeably, compared with the alloys Be20%-2 mm and Be32%-2 mm, the serrated flow behavior of the alloys, Be24%-2 mm and Be28%-2 mm, demonstrates two obvious characteristics: (i) The rheological stress drops of serrated flow are more concentrated in micro-stress drop zones. (ii) There are more stress drops per unit decreasing amplitude of reduced stress. These two evident phenomena in serrated flow behavior correspond to their high compressive plasticity.

Table 1. Mechanical properties of the glassy samples of $(Zr_{40}Ti_{40}Ni_{20})_{100-x}Be_x$ ($x = 20, 24, 28, 32$).

x_{Be}	σ_y (MPa)	ε_p (%)	ε_{max} (%)	σ_{max} (MPa)
20	1850	7.37	10.2	2125
24	1939.7	13.35	16	2174
28	1781	11.5	14.3	2111
32	1351	5.6	7.5	1403

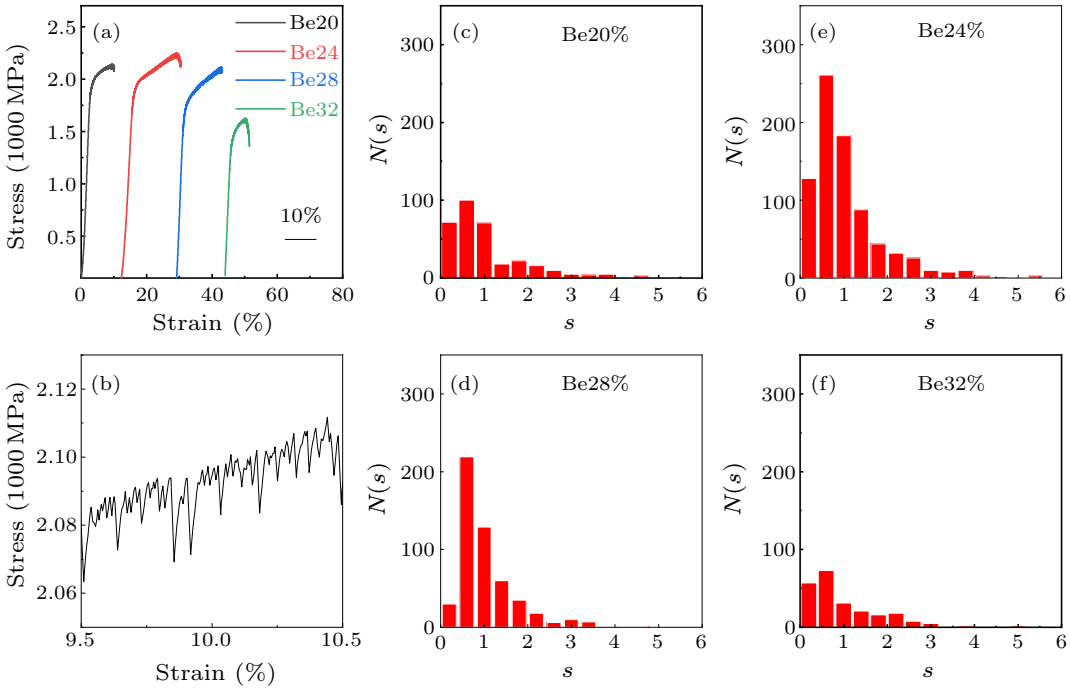


Fig. 2. (a) Stress–strain curves of completely MG samples with diameter of 2 mm; (b) serrated flow behavior of Be24%-2 mm in the strain region between 9.5% and 10.5%; (c)–(f) distribution histograms of the magnitude of the stress drop for the MGs of Be20%-2 mm, Be24%-2 mm, Be28%-2 mm, and Be32%-2 mm, among which the lateral axis s represents the decreasing amplitude of reduced stress in the sawtooth rheological curve, while the longitudinal axis $N(s)$ represents the number of stress drops corresponding to the decreasing amplitude of reduced stress s.

The stress-strain curves in Fig. 2(a) indicate that the four MGs all exhibit distinct work-hardening behavior as a result of factors such as intersection and interactions of multiple shear bands.[35] Figures 3(a), 3(b), and 3(c) show the SEM images of the profile, enlarged shear band distribution and fracture morphology of the compressed glassy samples of Be20%-2 mm, Be24%-2 mm, Be28%-2 mm, and Be32%-2 mm. To reveal the fracture mechanism of these alloys, an SEM was used to explore the fracture morphologies of Be20%-2 mm, Be24%-2 mm, Be28%-2 mm, and Be32%-2 mm, with the results shown in Fig. 3. As shown in Figs. 3(a-1), 3(b-1), 3(c-1) and 3(d-1), the two glassy samples with excellent plasticity (Be24%-2 mm and Be28%-2 mm) both present significant bulging.[35] Meanwhile, no obvious change is manifest in the profiles of the compressed samples with low plasticity (Be20%-2 mm, and Be32%-2 mm). Correspondingly, dense shear bands are formed on the surfaces of the two plastic amorphous samples; bending appears at the shear bands to a certain extent, significantly increasing the difficulty of the shear-band extension to increase the stress borne by the samples. The increased stress again stimulates the generation of shear bands. Figures 3(a-2) and 3(b-2) show the intersecting dislocations arising between primary and secondary shear bands: some of the shear bands show evident bending; while shear bands are not completely parallel, with different spacings therein; some shear bands exhibit a bifurcation phenomenon. The derived small shear bands or other shear bands intersect, or gradually vanish with gradual diffusion. These primary and secondary densely distributed and interacted shear bands lead to the inhibition of nucleation and extension of cracks.[36–38] On the contrary, these characteristics are not manifest in the sparsely distributed shear bands on the surface of the compressed sample of Be20%-2 mm and Be32%-2 mm, especially for Be32%-2 mm. As illustrated in Figs. 3(b-3) and 3(c-3), the fracture surfaces of two samples are both covered by typical veined patterns. These morphologies arise from the elastic strain energy accumulated in shear bands under the effect of gravitational action.[39] In addition to veined patterns, there are also some plat sites present in the fracture morphologies of the samples of Be20%-2 mm and Be32%-2 mm. Generally, the larger the density of veined patterns, the better the plasticity of amorphous alloys.[40] Hence the fracture morphologies of the samples conform well to their compression performances.

According to Chen *et al.*, the free volume of MGs exerts important influences on the formation, propagation, and bifurcation of shear bands.[41] Meanwhile, free volume also increases the atomic mobility, therefore the increment of free volume is beneficial to improving the plasticity of MGs. Beukel *et al.* found that the content of free volume in MGs can be characterized by relaxation enthalpy of amorphous alloys.[42] A thermal analysis of four MG rods with diameter of 2 mm was conducted to measure their relaxation enthalpy. As illustrated in the DSC heating curves (Fig. 4(a)), an exothermic process occurs before glass transition. As shown in shaded parts of Fig. 4(a), the quantity of heat released in this process is deemed equivalent to the relaxation enthalpy. The relaxation enthalpy values of the four MGs (Be20%, Be24%, Be28%, and Be32%) are 2.5 J/g, 4.9 J/g, 3.6 J/g, and 0.9 J/g, respectively. Figure 4(b) displays a quasi-linear correlation between relaxation enthalpy and plastic strain in MGs: the larger the relaxation enthalpy, the greater the plastic strain, and the better the plasticity of such amorphous alloys.

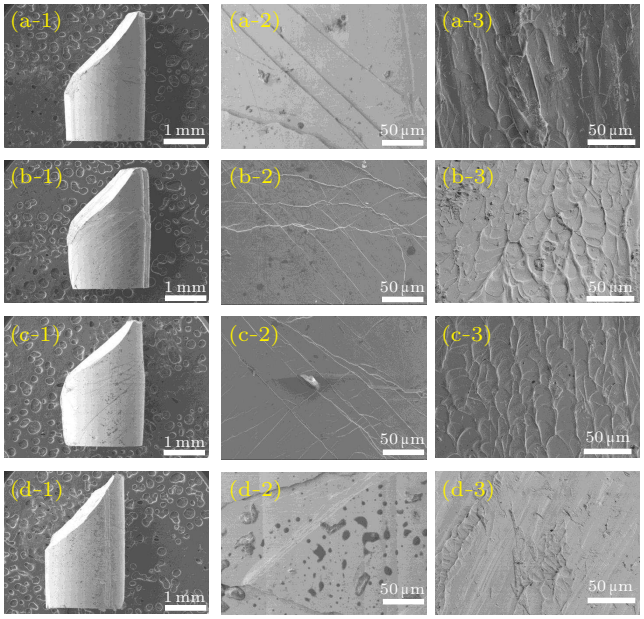


Fig. 3. (a)–(c) SEM images of the profile, enlarged shear band distribution, and fracture morphology of the compressed glassy samples of Be20%-2 mm, Be24%-2 mm, Be28%-2 mm, and Be32%-2 mm.

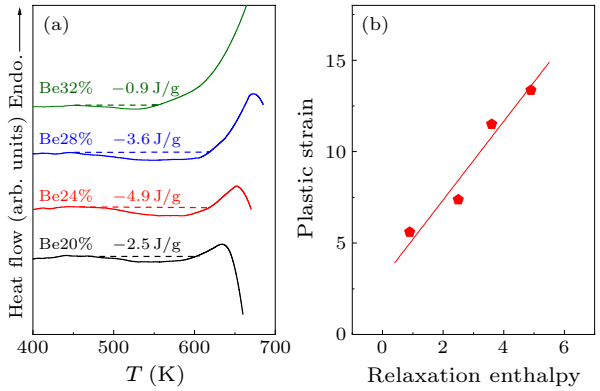


Fig. 4. (a) Heating DSC curves of the as-cast completely glassy rod with diameter 2 mm. The shadow zones correspond to relaxation enthalpy of amorphous alloys; (b) relationship between the relaxation enthalpy and plastic strain in the four MGs.

4. Conclusion

Through doping with Be in the icosahedral quasicrystalline alloy ($Zr_{40}Ti_{40}Ni_{20}$), four bulk MGs with better compressive plasticity were prepared with the following compositions: $(Zr_{40}Ti_{40}Ni_{20})_{100-x}Be_x$ ($x = 20$, 24, 28, 32). The

findings indicate that, except for the Be32% alloy, the quasi-crystalline phase is the main competitive phase of glassy phase, meaning that an icosahedral local order is one of the primary atomic configurations in these MGs. It is realized that the serrated flow behaviors of strain-stress curves for the Be24% and Be28% alloys both present near-exponential distributions. The primary and secondary shear bands are characterized by intersection, bifurcation, bending, etc. The fractures of both the glassy samples are densely distributed with typical veined patterns, which coincides with their high-plastic strain ($> 10\%$). The results imply that there is a quasi-linear relationship between the relaxation enthalpy and plastic strain in MGs: the greater the relaxation enthalpy, the larger the plastic strain.

Acknowledgments

This work was supported by the National Key R&D Program of China (Grant No. 2018YFA0703602), the National Natural Science Foundation of China (Grant Nos. 51871193, 52271155 and 52271154), the Natural Science Foundation for Excellent Young Scholars of Hebei Province (Grant No. E2021203050), the Hundred Talent Program of Hebei Province (Grant No. E2020050018), and the Hebei Province Innovation Ability Promotion Project (Grant No. 22567609H).

References

[1] Bruck H A, Rosakis A J and Johnson W L 1996 *J. Mater. Res.* **11** 503
[2] Inoue A 2000 *Acta Mater.* **48** 279
[3] Inoue A, Shen B L, Yavari A R and Greer A L 2003 *J. Mater. Res.* **18** 1487
[4] Inoue A, Shen B L and Chang C T 2006 *Intermetallics* **14** 936
[5] Lewandowski J J and Lowhaphandu P 1998 *Int. Mater. Rev.* **43** 145
[6] Wang W H, Dong C and Shek C H 2004 *Mater. Sci. Eng. R* **44** 45
[7] Greer A L 1995 *Front. Mater. Sci.* **267** 1947
[8] Spaepen F 1977 *Acta Metall.* **25** 407
[9] Zhang Y and Greer A L 2006 *Appl. Phys. Lett.* **89** 071907
[10] Donovan P E and Stobbs W M 1981 *Acta Metall.* **29** 1419
[11] Johnson W L 1999 *MRS Bull.* **24** 42
[12] Zhang Y, Wang W H and Greer A L 2006 *Nat. Mater.* **5** 857
[13] Bei H, Xie S and George E P 2006 *Phys. Rev. Lett.* **96** 105503
[14] Liu Y H, Wang G, Wang R J, Zhao D Q, Pan M X and Wang W H 2007 *Science* **315** 1385
[15] Zhang B, Zhao D Q, Pan M X, Wang R J and Wang W H 2006 *Acta Mater.* **54** 3025
[16] Liu Y H, Wang D, Nakajima K, Zhang W, Hirata A, Nishi T, Inoue A and Chen M W 2011 *Phys. Rev. Lett.* **106** 125504
[17] Peng H L, Li M Z and Wang W H 2011 *Phys. Rev. Lett.* **106** 135503
[18] Qiao J, Zhang L, Tong Y, Lyu G, Hao Q and Tao K 2022 *Adv. Mech.* **52** 117
[19] Zhu Z W, Gu L, Xie G Q, Zhang W, Inoue A, Zhang H F and Hu Z Q 2011 *Acta Mater.* **59** 2814
[20] Ding J, Cheng Y Q and Ma E 2014 *Acta Mater.* **69** 343
[21] Zhou W, Lin X and Li J F 2013 *J. Alloys Compd.* **552** 102
[22] Setyawan A D, Saida J, Kato H, Matsushita M and Inoue A 2010 *Intermetallics* **18** 1884
[23] Pan J, Chan K C, Chen Q and Liu L 2012 *Intermetallics* **24** 79
[24] Ren H T, Pan J, Chen Q, Chan K C, Liu Y and Liu L 2011 *Scr. Mater.* **64** 609
[25] Liu L, Chan K C, Sun M and Chen Q 2007 *Mater. Sci. Eng. A* **445** 697
[26] Saida J, Matsushita M, Li C and Inoue A 2000 *Appl. Phys. Lett.* **76** 3558
[27] Saksl K, Franz H, Jóvári P, Klementiev K, Welter E, Ehnes A, Saida J, Inoue A and Jiang J Z 2003 *Appl. Phys. Lett.* **83** 3924
[28] Louzguine D V and Inoue A 2001 *Appl. Phys. Lett.* **78** 1841
[29] Qiang J B, Wang Y M, Wang D H, Kramer M, Thiel P and Dong C 2004 *J. Non-Cryst. Solids* **334** 223
[30] Li Z, Pan S, Zhang S, Feng S, Li M, Liu R, Tian Y and Wang L min 2019 *Intermetallics* **109** 97
[31] Cahn J W, Shechtman D and Gratias D 1986 *J. Mat. Res.* **1** 13
[32] Qiang J B, Wang Y M, Wang D H, Kramer M, Thiel P and Dong C 2004 *J. Non-Cryst. Solids* **334** 223
[33] Li Z J, Zhao L R, Pan S P, Fan C Z, Qiang J B, Dong C and Wang L M 2018 *J. Alloys Compd.* **746** 356
[34] Sun B A, Yu H B, Jiao W, Bai H Y, Zhao D Q and Wang W H 2010 *Phys. Rev. Lett.* **105** 035501
[35] Das J, Tang M B, Kim K B, Theissmann R, Baier F, Wang W H and Eckert J 2005 *Phys. Rev. Lett.* **94** 205501
[36] Abelson P H 1987 *Science* **235** 9
[37] Xi X K, Zhao D Q, Pan M X, Wang W H, Wu Y and Lewandowski J J 2005 *Phys. Rev. Lett.* **94** 125510
[38] Greer A L, Cheng Y Q and Ma E 2013 *Mater. Sci. Eng. R* **74** 71
[39] Trexler M M and Thadhani N N 2010 *Prog. Mater. Sci.* **55** 759
[40] Zhou M, Hagos K, Huang H, Yang M and Ma L 2016 *J. Non-Cryst. Solids* **452** 50
[41] Chen L Y, Setyawan A D, Kato H, Inoue A, Zhang G Q, Saida J, Wang X D, Cao Q P and Jiang J Z 2008 *Scr. Mater.* **59** 75
[42] Beukel A and Sietsma J 1990 *Acta Metall. Mater.* **38** 383